Why this location

Newhaven port was selected as a demonstration site as an additional UK south coast study site. The port also has significant coverage of steel pile walling and other marine steel constrcution, but in contrast to the Shoreham demonstration site consists of an estuarine channel open to the sea. The site therefore represents a signifcant commercial port facility, with both similarities and contrast to the site selected at Shoreham. This was planned to allow comparison and generalisation of the results.

Baseline/starting situation

Newhaven Port, is an active commercial and passenger port facility on the mouth of the River Ouse, West Sussex, UK (Figure NH1). Bed sediment is dominantly of silt grade quartz and calcite, with kaolinite and illite clays and a significant organic content. The port area has at least 3km of steel pile wall. The sampling location was adjacent to the site office at 50°47’02”N, 0°03’27”E, within the intertidal zone accessible at low tide. Sediment samples were taken from the opposite side of the harbour accessible around fishing boat moorings. The SOCORRO monitoring system was installed on the East Pier at 50°46’57”N, 0°03’28”E. Additional access and support for sampling and installations was provided by the Port Authority through use of the port pilot boat.

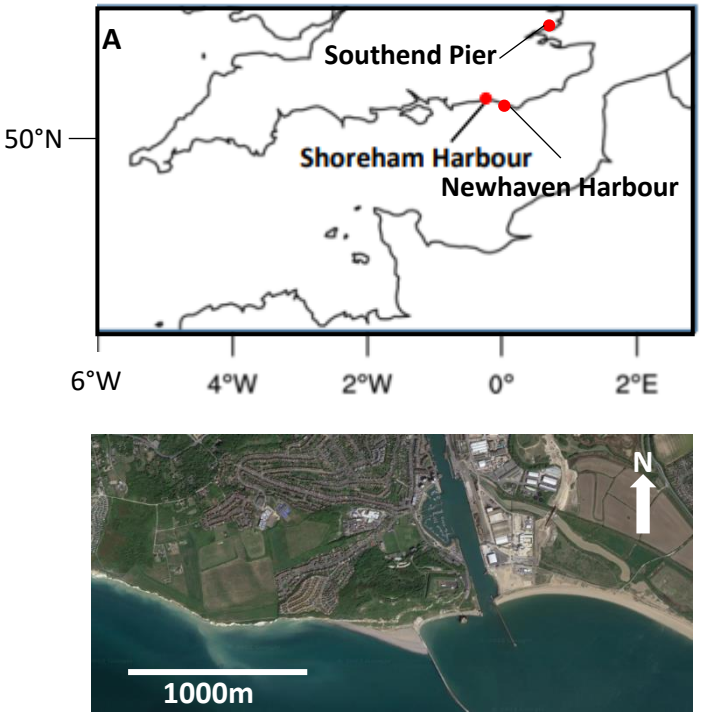

Figure NH1: Location and Google Earth Image of Newhaven Harbour.

The Newhaven site had a program of baseline environmental sampling from November 2020 to July 2021. The sampling included corrosion, water and sediment cores used for solid sediment analyses, and pore water analyses. Sub-samples of each sample type were taken for microbial analyses (detailed in the Shoreham demonstration site report) as these sites are subject to microbiologically influenced corrosion (Accelerated Low Water Corrosion). Samples were collected either from intertidal sites, from the port side, or accessed via the Port Authority inshore pilot boat. Images of steel corrosion, the sampling procedure and corrosion are given in Figure NH2.

Figure NH2: Images of Newhaven Port environment and corrosion. (A) View of the steel pile wall. (B) Water and corrosion sampling from pilot boat. (C) Corrosion sampling from pilot boat. (D) Removed intertidal corrosion blisters show inner sulphidic layer and acid etched steel.

The results of mineralogical and chemical analysis of corrosion samples are shown in Figure NH3. The FTIR spectra are characterised by a broad adsorption peak from 3000-3500cm^{-1} that can be attributed to O-H groups and H_20, and multiple complex peaks in the range 600-1800cm^{-1}. Analysis of FTIR spectra was concentrated in the latter range as these absorption bands can be related to corrosion products on the steel surface. Two areas of the spectra were interpreted in detail using the PeakFit 4.12 software to deconvolute composite absorption peaks. Peaks were identified using

gaussian amplitude deconvolution with a second derivative-based background fit, in separate windows from 750-1200cm^{-1} and from 1250-1750cm^{-1}. Deconvolution used a fixed full width at half maximum peak height of 18.1cm^{-1}, except for visibly narrower peaks at 861cm^{-1} and 874cm^{-1} where FWHM was reduced to fit the visible peaks. Within the intertidal corrosion samples lepidocrocite absorbance peaks at 746cm^{-1} and 1023cm^{-1} were developed in all samples (RRUFF database). Within the Newhaven samples absorption peaks at 781cm^{-1}, 841cm^{-1}, and 874cm^{-1}, can be attributed to Fe-OH stretching modes in sulphate green rust (Peulon et al., 2003). Peaks at 992cm^{-1}, 1095cm^{-1}, 1109cm^{-1}, and 1156cm^{-1} can be attributed to various SO_4^{2-} vibration modes in green rust ((Borda et al., 2004; Peulon et al., 2003; Rouchon et al., 2012) and that at 874cm^{-1} may also be influenced by HSO_4^- (Usher et al., 2005). The sulphur species vibrational modes are not well developed in SE6, indicating a lack of sulphur compounds in this sample. The broad adsorption band from 1250-1550cm^{-1}, can be deconvoluted to peaks from ferric and ferrous hydroxide gel at 1339cm^{-1} and 1396cm^{-1} (Chernyshova, 2003), those at 1435cm^{-1} and 1473cm^{-1} to the presence of carbonate from calcite or aragonite shell material (RRUFF database), and that at 1519cm^{-1} to the O-H bond deformation. The peak at 1627-1637cm^{-1} can be attributed to water (Shahabi-Navid et al., 2020). It should be noted that the presence of biofilms in intertidal samples means that spectra may be influenced by the presence of polysaccharide biofilms on the surface (Beech et al., 2005; Zinkevich et al., 1996). We have tested for this using the spectra of reagent grade alginic acid and sodium alginate (both components of marine biofilm extra cellular polymeric substances (EPS) (Beech and Sunner, 2004; Sachan and Singh, 2020). These have characteristic absorption bands at 1244cm^{-1} and 1598cm^{-1} respectively which are absent from the samples (Figure NH3 A). The sulphate adsorption bands arise from the formation of sulphate green rust by sulphide oxidation as part of the MIC mechanism and could be used as a rapid diagnostic tool of accelerated microbially influenced corrosion types.

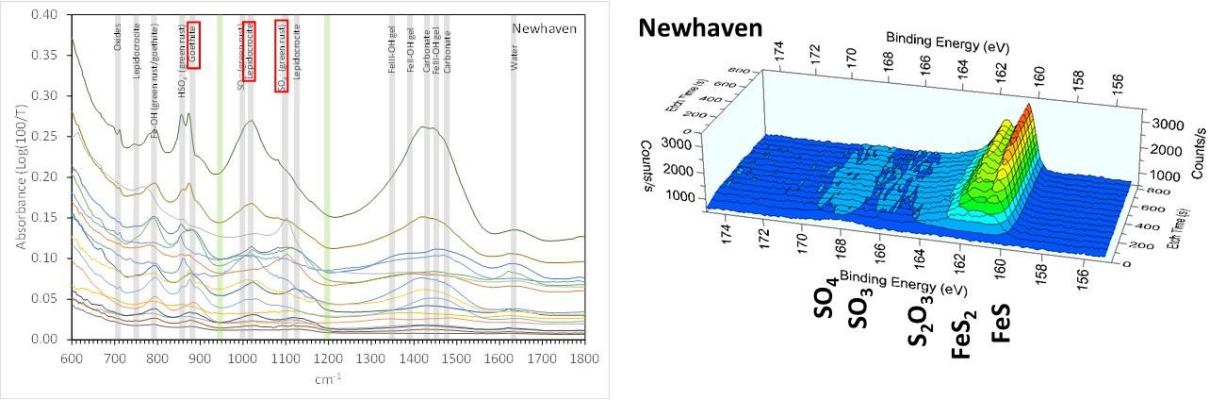

Figure NH3: Results of corrosion characteristion, Newhaven Port. (A) Fourier transform infrared spectra of corrosion products. In this case dominated by iron oxides and oxy-hydroxides alongside sulphate. (b) X-ray photoelectron spectrum of intertidal corrosion products. Sulphides and sulphate are detectable in corrosion products.

Infrared spectroscopy was been supplemented by X-ray photoelectron spectroscopy on selected samples to confirm the detailed corrosion mechanism. This technique is not suited for rapid diagnosis of corrosion type and hazard due to complexity and cost, but provides detailed information on the chemistry of corrosion products which can be used to confirm interpretations of corrosion mechanism from other techniques. This gives a firm basis for the utilisation of rapid low cost mineralogical techniques in the analysis of corrosion type. This is particularly useful for instances of microbially influenced corrosion which may lead to high corrosion rates with significant hazard to infrastructure. XPS depth profiles show the red outer surface of corrosion blisters have lower Fe content compared to the interior. In the outer, red portion Fe varies from 10-30 atom %, and in the inner, black portion it varies from 3-6 atom %. Detailed interpretation of the sulphur 2p3/2 peak indicate sulphur is dominated by sulphate on the corrosion surface, with minor components of sulphite and thiosulphate developed with depth into the sample. The interior of the sample is dominated by iron sulphides (Figure NH3 B). This confirms the accelerated low water corrosion mechanism as the production of hydrogen sulphide at the steel surface by sulphate reducing bacteria. This reacts with iron to produce iron sulphides. These are then oxidised by iron oxidising and sulphur oxidising bacteria, ultimately producing sulphate compounds. Acidity is generated at every stage, account for the highly corrosive microenvironment. A strong conclusion form this is that sulphur compounds detectable by simple spectroscopic techniques can be used as diagnostic of microbially influenced corrosion, which can then inform the SOCORRO corrosion risk assessment methodology.

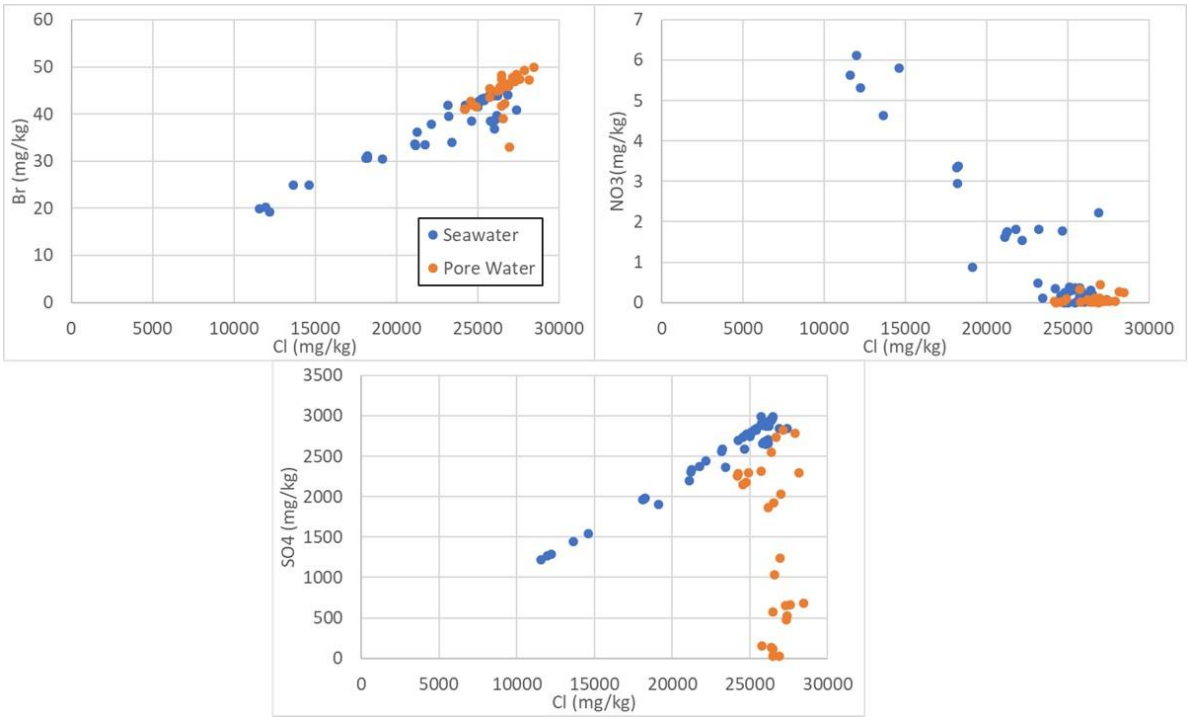

Figure NH4: Anion chemistry of sea/estuarine water and sediment porewater from Newhaven.

The environment surrounding the marine steel work was monitored in order to inform the subsequent continuous monitoring program, and to identify risk factors for microbially influenced corrosion. The anion chemistry of seawater is shown in Figures NH4 and NH5. The bromide and chloride concentrations are strongly correlated in both seawater and sediment porewater, consistent with fully marine water diluted by river water. This is typical of estuarine systems. Nitrate is most strongly concentrated in low salinity water. Nitrate is a nutrient contaminant, and has been previously implicated in the generation of ALWC/MIC through encouraging biofilm growth. The negative correlation with chloride concentration indicates that the main nutrient input is from river water in the estuarine system. Sulphate correlates strong with chloride in seawater, and this reflects the same trend of seawater dilution by river water. However, sediment porewaters depart strongly from this trend, extending to very low sulphate concentrations. This indicates the action of sulphate reducing bacteria in the sediment, confirming anoxic bed sediment as a reservoir of causative bacteria for MIC, and identifying an environmental risk factor for accelerated corrosion types that can be used in hazard assessment.

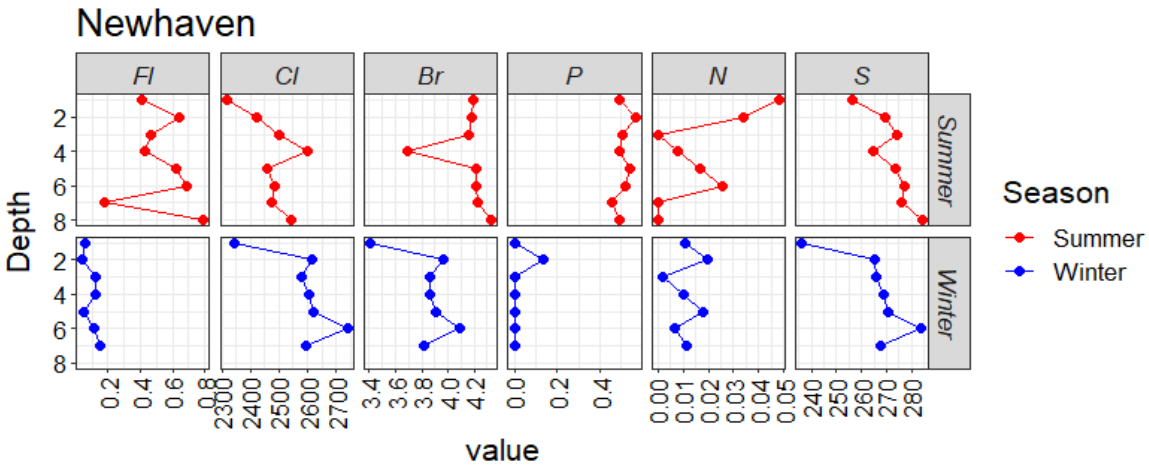

Figure NH5: Depth profiles in water column for anion chemistry from Newhaven.

Figure NH5 shows summer and winter season depth profiles for the port water column anion concentration. All anions reflect the estuarine environment – low concentration river water occurs on top of saline marine water due to its lower density. The exception to this nitrate during the summer period, where lower rain fall means higher nitrate concentrations in onshore run off because of lower dilution by rainfall. There is strong seasonality in nutrient inputs to the port environment which may influence biological activity.

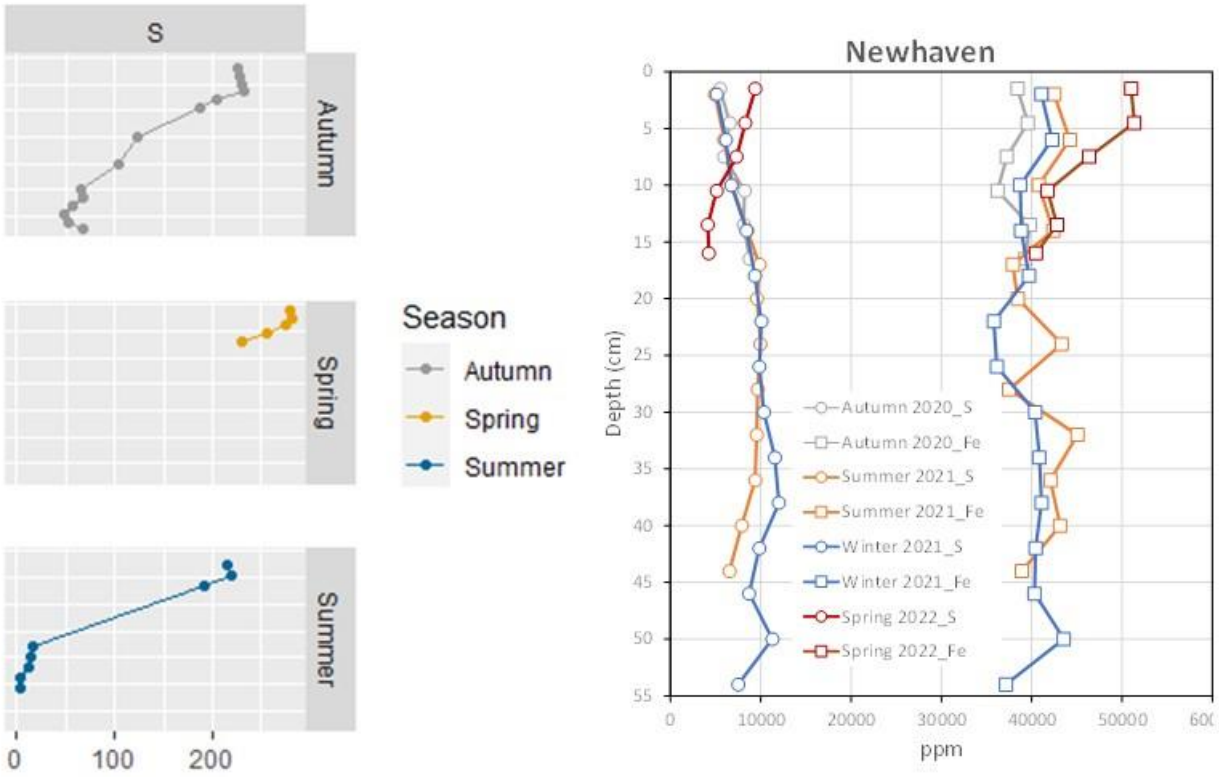

Figure NH6: Depth profiles of pore fluid (left solid phase iron and sulphur content (right) from sediment cores at Newhaven.

Analysis of sediment cores included solid phase iron and sulphur, and porewater iron and sulphur, sampled over 4 seasons. During all seasons the sulphate content in pore water declines rapidly with depth (Figure NH6). In autumn, winter and summer the solid iron and sulphur contents increase with depth. Taken together with the pore water chemistry these are an indicator of the action of sulphate reducing bacteria in the bed sediment, using sulphate from pore water and generating iron sulphide minerals, and support bed sediment anoxia as a potential risk factor for MIC. This has further been confirmed by comparison of sediment and corrosion microbiology detailed in the demonstration site report on Shoreham Port. A reduction in solid state sulphur and iron in summer 2022 can be related to high freshwater flows at the end of the winter period resulting in sediment redistribution.

Construction

Continuous monitoring of water chemistry parameters and corrosion rate was conducted in Newhaven Port from 2nd to 22nd December 2022. The equipment installed was an Aquaread AP6000 multiparameter probe, with sensors for temperature (T), water electrical conductivity (Cond.), pH, oxidiation-reduction potential (ORP) and chlorophyll. The AP6000 includes an automatic cleaning head

which is important for marine applications to prevent obstruction of the senors by biofouling and sediment build-up. The AP6000 was powred by solar panel an linked to a data logger with a Point Orange mobile phone uplink to allow remote download of data via the internet. The AP6000 was programmed to record data every hour. Corrosion rate was monitored using CCube linear polarisation resistance sysem, powered by a solar panel, and enabled for remote dowload of data by an additional mobile phone uplink. The intitial plan was to install the system adjacent to steelwork in the active part of the port. However, issues with multiple ownership (parts of Newhaven Port are owned by the Port of Dieppe and the ferry operator), and concerns around the 4G mobile phone systems interferring with port monitoring equipment, including the port radar, meant this was not possible. The equipment was therefore installed from the east pier (visible in Figure NH1) at the mouth of the port and harbour area.

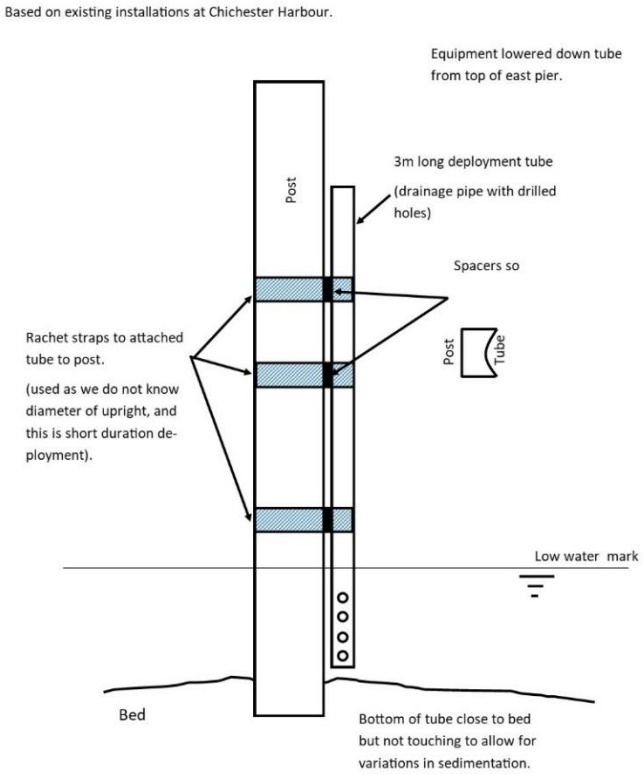

Figure NH7: Design of SOCORRO installation at Newhaven Port.

The sensors were deployed via drainpipes with pre-drilled holes to allow free circulation of water, secured to the pier upright supported by ratchet straps (Figure NH7). The pipes were installed from the Port pilot boat at low tide. Additional ratchet straps were added to further secure the pipes at high tide. The data loggers and solar panels were secured to the pier railings (Figure NH8). Unfortunately, a combination of a spring high tide and winter storm swell broke the installaion loose on the 22nd December. All equipment was recovered intact, but could not be re-deployed as it became apparent

the CCube system had a design fault. The manufacturers solution to this could not be implemented as the unit had been supplied with a faultly USB chip, such that new control software could not be installed. It consequently had to be returned to the manufacturers for upgrade, and wasnot returned in time for re-installation before the end of the project.

The installation site at Newhaven was not ideal becuase of the exposed position and high water flows. Future deployments would be facilitated by clear documentation from equiment manufacturers detailing equipment output frequencies, so that inference risks with existing monitoring infrastructure can be evaluated.

Figure NH8: Photographs of the final installation, Newhaven Port.

Results:

Time series plots from 8th to 22nd December of all monitored data are shown in Figures NH9 and NH10. The means and ranges of data are shown in Figure NH11. The data are strongly tidlly influenced, and a portion of one spring to neap tidal cycle in water depth(calculated from water pressure) was captured by tge monitoring period. These cycles influence all other variables. In terms of depth notably on spring low tides the steel piling and the monitoring point can be exposed to atmosphere. Temperature varied between 0-10°C, with with low T corresponding to exposure to atmosphere at night time. Dissolved oxygen also varied tidally, but only to minor extent excpet for when the steel was atmospherically explosed on low tide (Figure NH11). Oxidation-reduciton potential (ORP) shows variaiton in relation to the diurnal nd monthly tidal cycle, with relative highs on sub-aerial exposure, and lows at hight T and low conducitvity (high freshwater input). pH is relatively constant between 7.6 and 8.15, with soem slight bimodality with the changing tide. Conductivity vaires bimodally in relation to the relative input of marine and freshwater through the tidal cycle in an estuarine environment. Chlorophyll is typically close to the detection limit of the sensor system, except for isolated peaks presumed to relate to the resuspension of algal material at spring low tides.

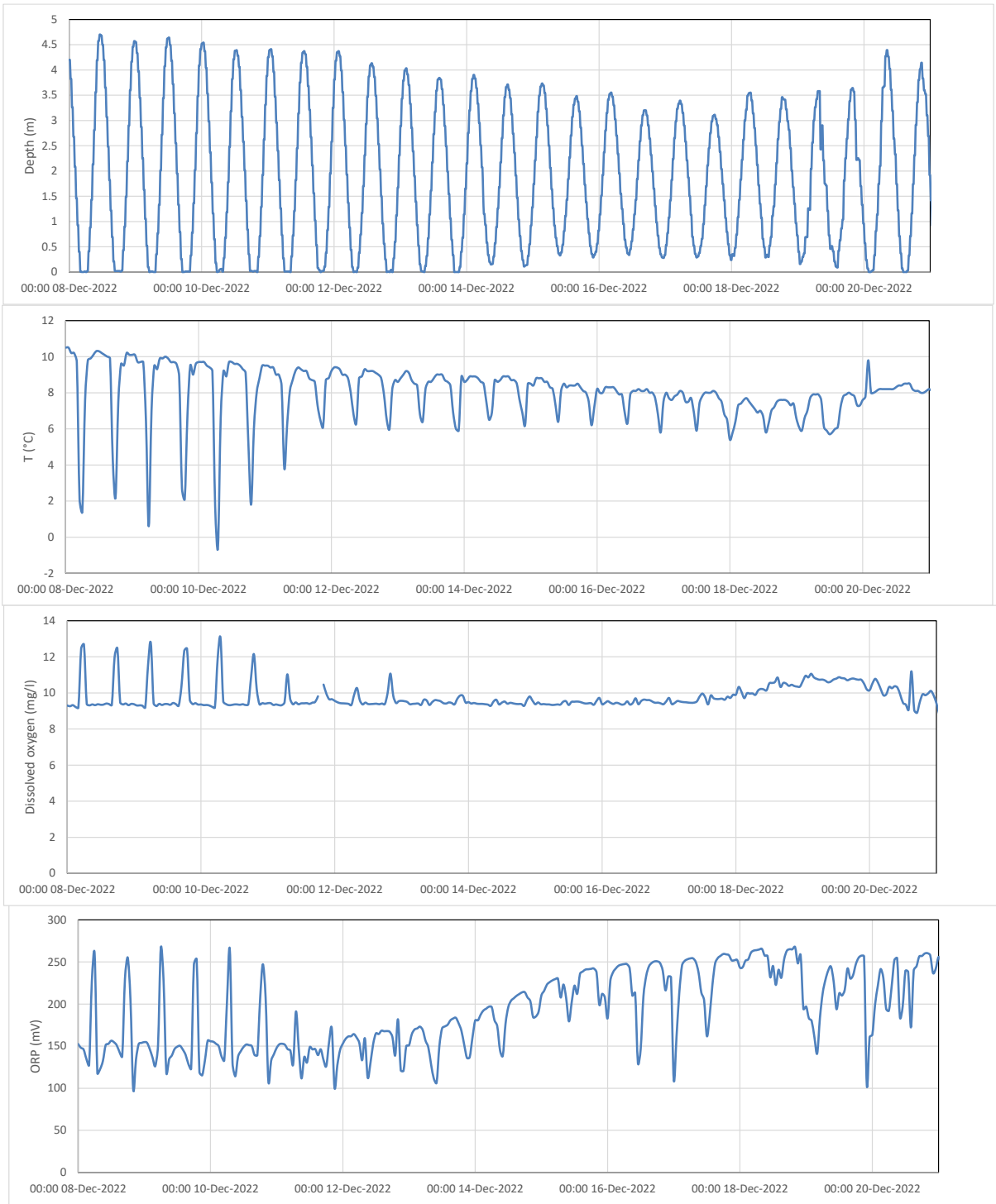

Figure NH9: Time series of water depth, temperature, dissolved oxygen and oxidation-reduction potential (ORP) from Newhaven East Pier.

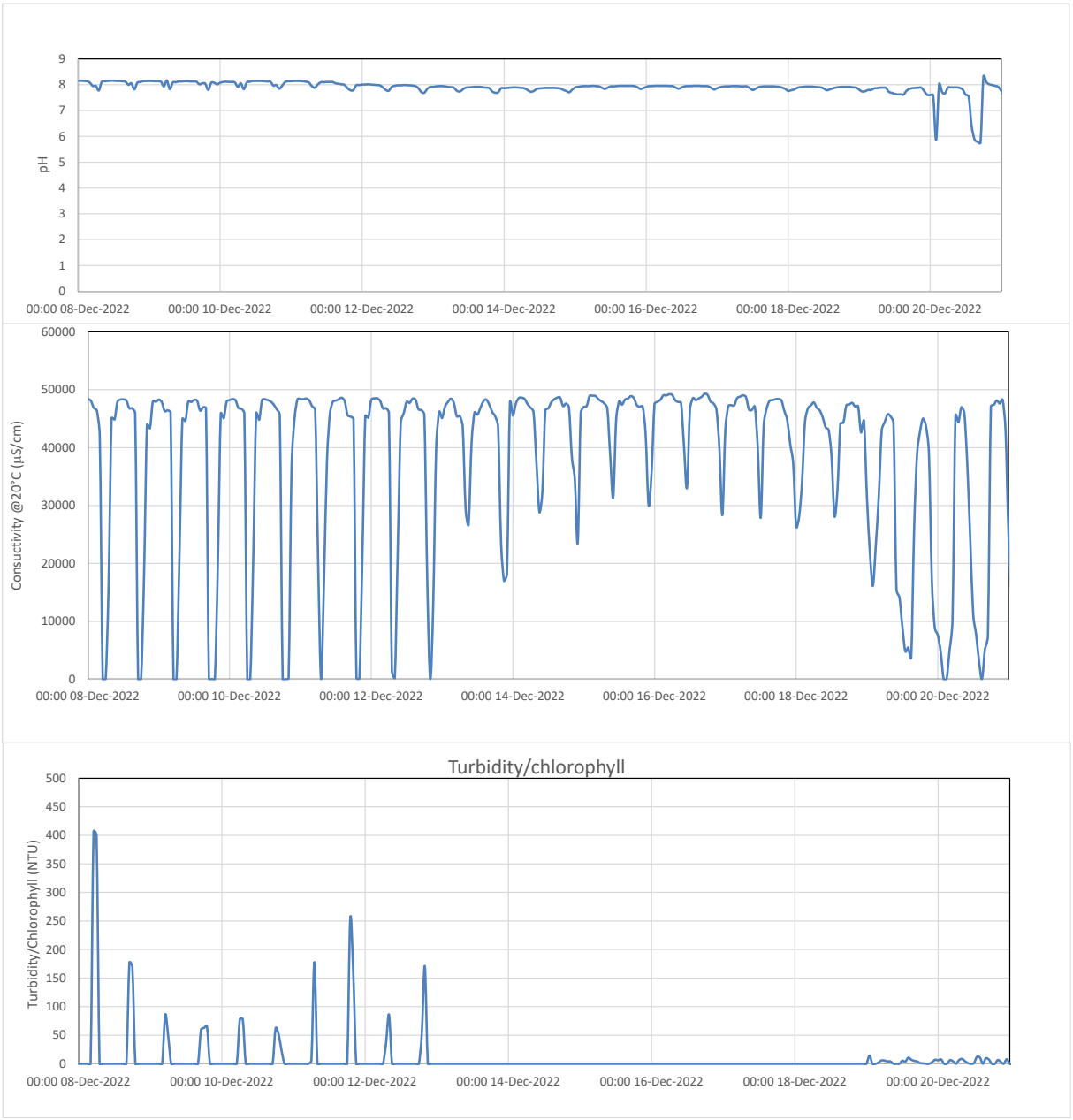

Figure NH9(continued): Time series of pH, conductivity and turbidity/chlorophyll from Newhaven East Pier.

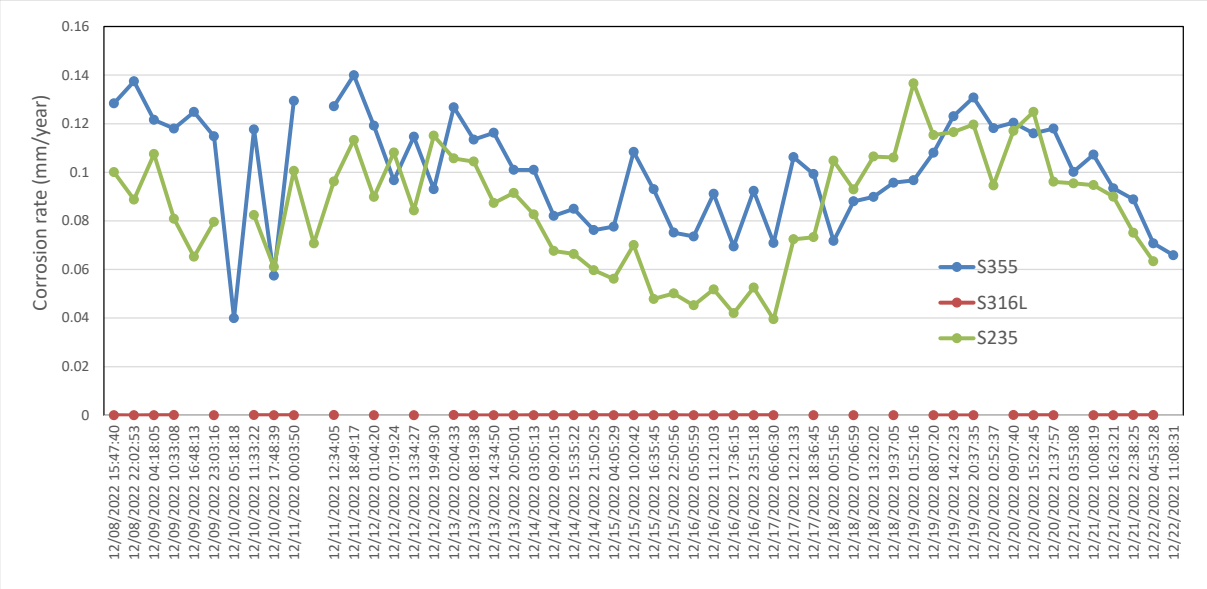

Figure NH10: Time series of corrosion rate in different steel grades from Newhaven East Pier CCube sensor.

The Corrosion rate at Newhaven varied between 0.04 to 0.14mm/year for S235 steel, from 0.05 to 0.14mm/year for S355 steel, and was typically below 0.01mm/year for S316L (stainless) steel. Bivariate correlation between corrosion rate and environmental parameters is particularly apparent with dissolved oxygen, temperature and depth (which drives variation in other parameters in a tidal environment) in both S235 and S355.

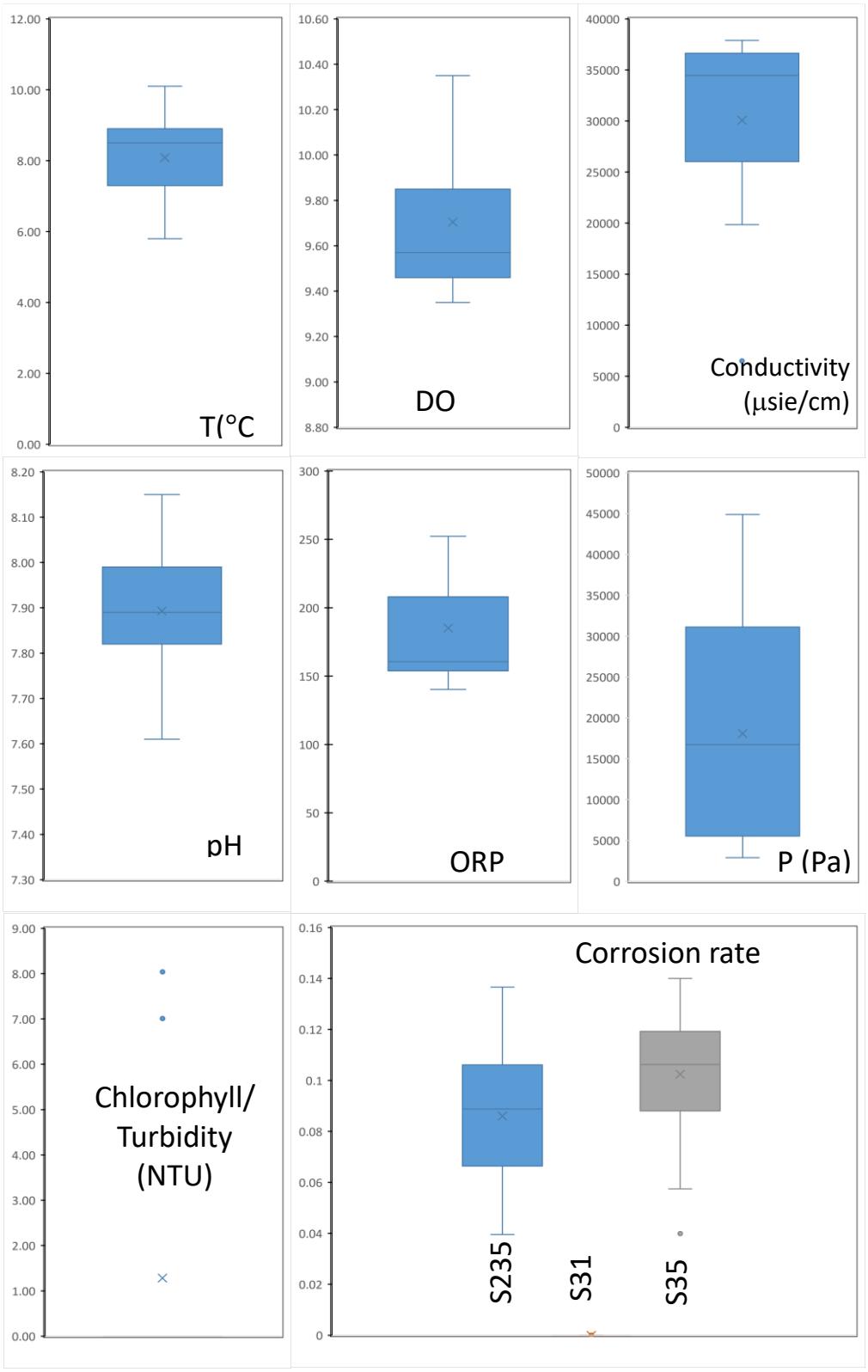

Figure NH11: Box and whisker plots indicating median, upper and lower quartiles and outliers for environmental parameters and corrosion rate.

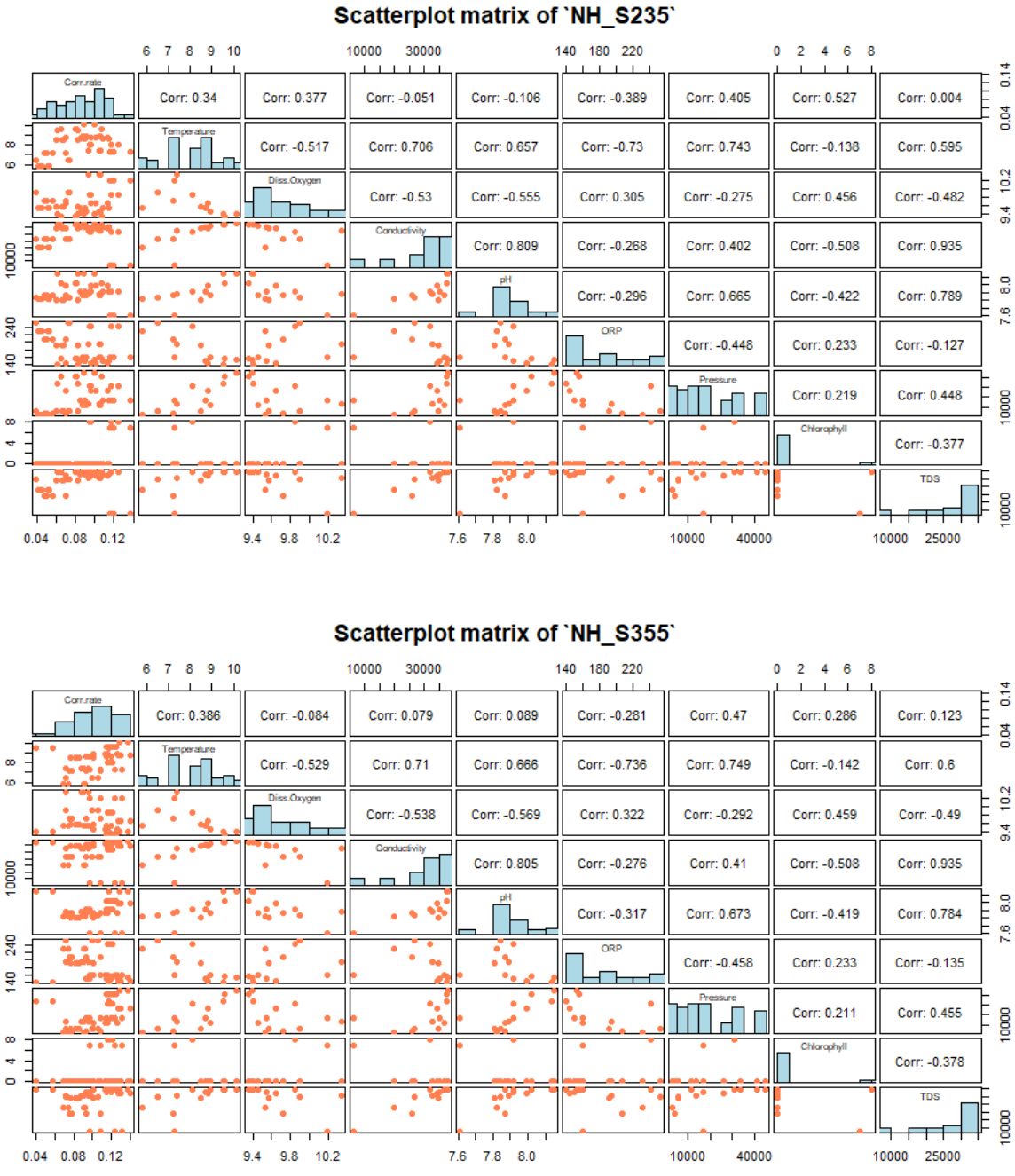

Figure NH12: Bivariate correlation plots and Pearson correlation co-efficients for S235 and S355 steel with environmental parameters.

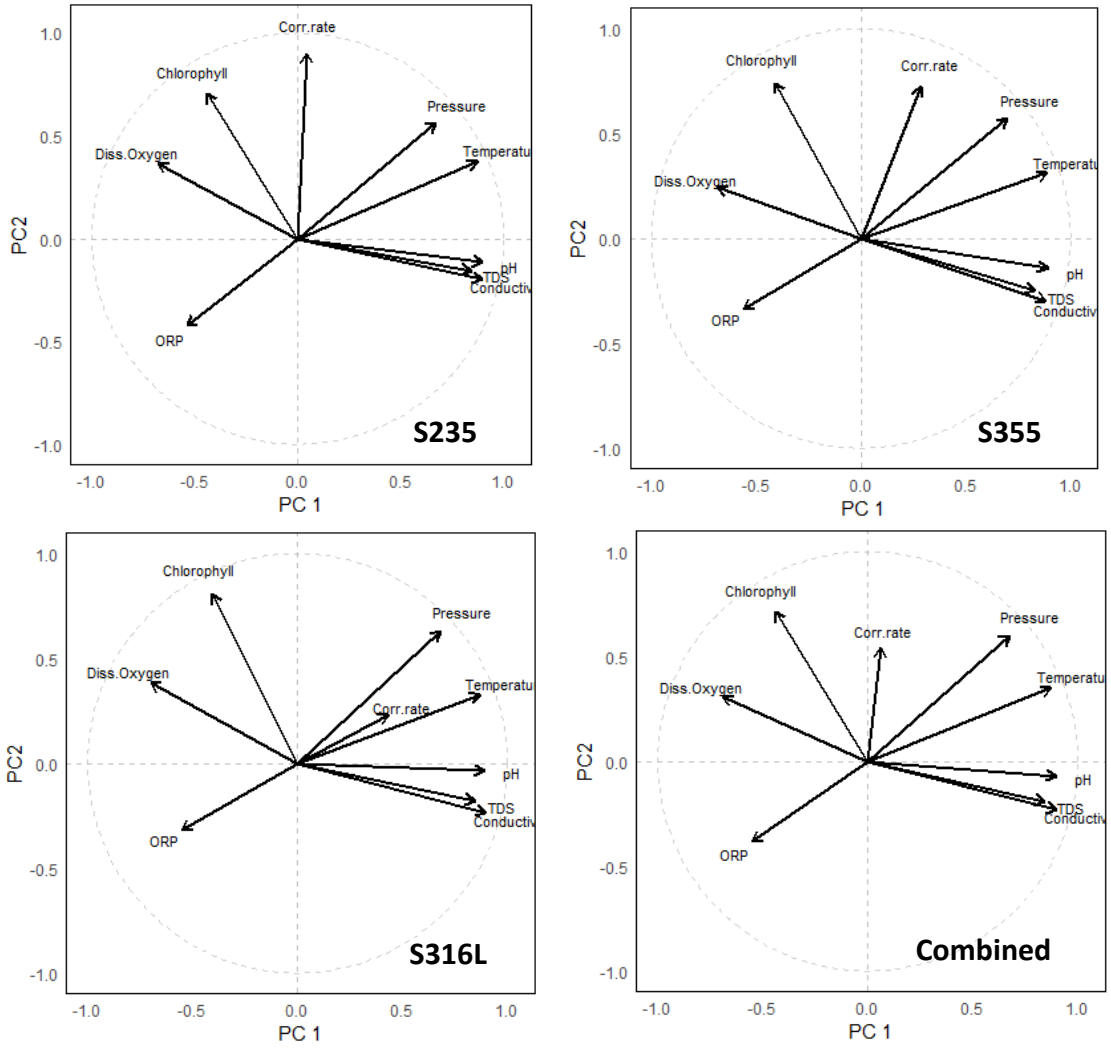

Figure NH13: Results of principal components analysis of corrosion rate and environmental parameters at Shoreham.

The data were also analysed using multivariate statistics via principal components analysis. The weightings of individual variables within the first 2 principle components at shown in Figure NH13. In all cases the majority of variation in the data is accounted for by conductivity, which varies with the relative fresh and marine water contributions in the tidal cycle. In both S235 and S355 PC1 (50.1% of variation) is dominated by variation in conductivity and dissolved oxygen, and PC2 (18.04% of variation) is dominated by corrosion rate. When the principal components are plotted against each other for each measurement point (Figure NH14) it is clear the highest corrosion rates (high PC2) correlate with high temperature and pH. However, as at Shoreham, PC2 is highest when PC1 is negative corresponding to the shallowest water, and highest dissolved oxygen .

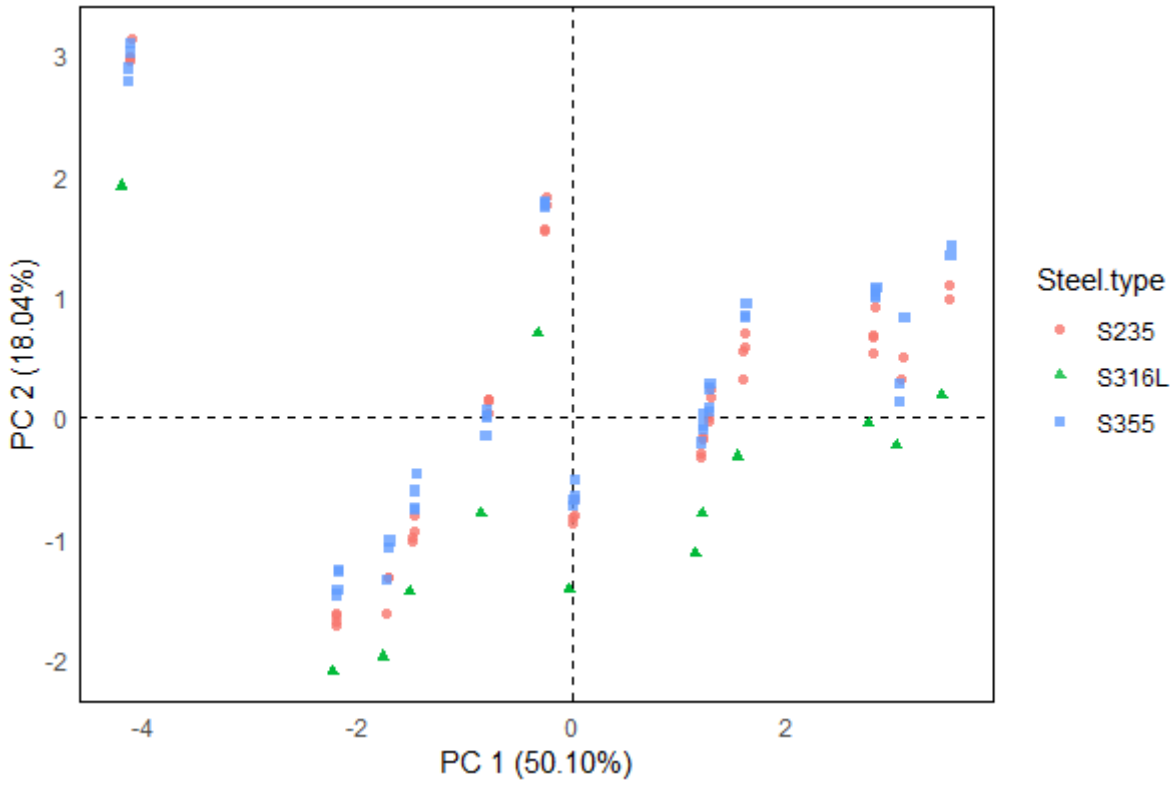

Figure NH14: Results of principle components analysis for each measurement time.

As at Shoreham, the statistical analysis shows that there are two regimes driving high corrosion rate. When the steel is fully immersed then corrosion rate correlates positively with temperature and pH. At low tide the exposure to atmospheric oxygen drives accelerated corrosion rate independently of temperature. These can be related to corrosion mechanism whereby temperature increase reaction rates during immersion, but corrosion reactions consume oxygen and are thus accelerated further during very low water and atmospheric exposure.

Figure NH15: Out put from the SOCORRO corrosion risk application. (A) Display of monitoring data. (B) Predicted corrosion risk. (C) Predicited corrosion risk averaged over a 10 hour period. (D) Cumulative corrosion risk. Thresholds of critical corrosion risk are arbitrarily set at 0.15 and the cumulative corrosion risk is set at 20 to demonstrate the visualisation capabilities.

Analysis of the monitoring data from Newhaven is shown in Figure NH15. The corrosion risk was predicted using the 'Seawater, Field Trained' algorithm, which is based on the July to September monitoring period at Shoreham. Corrosion risk is predicted to be highest at spring low tides, when the steel work is fully exposed to atmosphere. The periods of predicited high corrosion risk correspond to the measured periods of high corrosion from the CCube sensor, indicating the success of the approach. For the short period of immersion of the corrosion rates are not particularly high and and the risk is relatively low, but a threshold instaneous risk of 0.15 and an threshold accumlated risk of 20 have been used to illustrate the visualisation capabilities of the application.

Plans for further use?

The Newhaven installation could not be continued because of the issues detailed above. However, steel coupons for mass loss measurement are still deployed in the port and these will be recovered for measurement over the coming months. The ~1 month of monitoring data obtained will be analysed using the SOCORRO application, and the result shared with the Newhaven Port Authority, with a view to their supporting a re-installation of monitoring equipment in the future.

References

I.B. Beech, J.A. Sunner, K. Hiraoka, Microbe-surface interactions in biofouling and biocorrosion processes, International microbiology, 8 (2005) 157-168.

I.B. Beech, J. Sunner, Biocorrosion: towards understanding interactions between biofilms and metals, Current opinion in Biotechnology, 15 (2004) 181-186.

M.J. Borda, D.R. Strongin, M.A. Schoonen, A vibrational spectroscopic study of the oxidation of pyrite by molecular oxygen, Geochimica et Cosmochimica Acta, 68 (2004) 1807-1813.

I. Chernyshova, An in situ FTIR study of galena and pyrite oxidation in aqueous solution, Journal of Electroanalytical Chemistry, 558 (2003) 83-98.

S. Peulon, L. Legrand, H. Antony, A. Chaussé, Electrochemical deposition of thin films of green rusts 1 and 2 on inert gold substrate, Electrochemistry communications, 5 (2003) 208-213.

V. Rouchon, H. Badet, O. Belhadj, O. Bonnerot, B. Lavédrine, J.G. Michard, S. Miska, Raman and FTIR spectroscopy applied to the conservation report of paleontological collections: identification of Raman and FTIR signatures of several iron sulfate species such as ferrinatrite and sideronatrite, Journal of Raman Spectroscopy, 43 (2012) 1265-1274

R. Sachan, A.K. Singh, Comparison of microbial influenced corrosion in presence of iron oxidizing bacteria (strains DASEWM1 and DASEWM2), Construction and Building Materials, 256 (2020) 119438

M. Shahabi-Navid, Y. Cao, J.-E. Svensson, A. Allanore, N. Birbilis, L.-G. Johansson, M. Esmaily, On the early stages of localised atmospheric corrosion of magnesium–aluminium alloys, Scientific Reports, 10 (2020) 1-16.

RRUFF database. http://rruff.info/about/about_general.php

C.R. Usher, K.W. Paul, J. Narayansamy, J.D. Kubicki, D.L. Sparks, M.A. Schoonen, D.R. Strongin, Mechanistic aspects of pyrite oxidation in an oxidizing gaseous environment: An in situ HATR− IR isotope study, Environmental science & technology, 39 (2005) 7576-7584

V. Zinkevich, I. Bogdarina, H. Kang, M. Hill, R. Tapper, I. Beech, Characterisation of exopolymers produced by different isolates of marine sulphate-reducing bacteria, International Biodeterioration & Biodegradation, 37 (1996) 163-17